NASA-CR-203796

Micro- and macro-segregation during alloy solidification

A. Hellawell
Department of Metallurgical and Materials Engineering,
Michigan Technological University, Houghton, Michigan, U.S.A.

Introduction

To attempt a comprehensive review of this subject area, with all the ramifications and consequences associated with grain size and distribution is beyond the scope of this presentation. Therefore, to be more selective, there are some general comments about the application of microsegregation analyses, inasmuch as they can be used to model solidification behavior, followed by a discussion of those aspects of macrosegregation which are gravity induced.

Evidently, in solidification processing, as in most fields of activity, there is a current preoccupation with modeling, and if this can be done in a physically realistic and predictive manner for castings, the effort has revolutionary potential for quality control, automation, and innovative design (1,2). This idea is not altogether new and was pioneered for eutectic cast irons by Oldfield (3) some thirty years ago. At present, it is not obvious that predictive modeling of the overall process will be possible but some aspects of the problem are further advanced than others.

Thus there have been model analyses of heterogeneous nucleation processes during initial recalescence (4) and predictions of the columnar to equiaxed transition for simple binary alloys (e.g. 5-7), and most recently, attempts to combine heat flow analyses with nucleation and growth for alloys containing primary and eutectic constituents (e.g. 8-9). As regards analyses of microsegregation, these have probably been advanced to a level beyond our capabilities in handling other aspects of the process as a whole.

I. Microsegregation and Thermal Analysis

The basic equations for fractional crystallization are essentially textbook material; (e.g. 10,11) it is their application to real foundry conditions which requires attention.

With the assumption that the scale of solid + liquid phase distribution during solidification is too coarse to allow significant diffusional mixing in the solid state, but is sufficiently fine to accommodate complete mixing in the liquid, a simple mass balance gives the well known relation attributed to Scheil (12):

$$C_L = C_o f_L^{(k_o-1)}$$

for the composition of a residual liquid fraction, f_L, during the solidification of an alloy, C_o, in a diagram such as Fig. 1. In systems where the solid solubility is negligible, the solid/liquid distribution coefficient, $k_o \rightarrow 0$, and the expression becomes:

$$C_L = C_o / f_L$$

which is the same as the lever rule. In practice, of course, k_o is not exactly a constant, so that with extended solid solubility, using a constant k_o, the Scheil equation becomes increasingly inaccurate at high solid fractions, $f_s = 1 - f_L$, inevitably predicting C_s or $C_L \rightarrow \infty$ as $f_L \rightarrow 0$. However, if variations of k_o with composition are included, the equation conveniently expresses expected solid/liquid composition traces with respect to some local reference volume and coordinates within a casting, predicting the occurrence or fraction of eutectic or peritectic phases which literal interpretation of the equilibrium diagram cannot. Clearly, also, the relationship can be further developed by introducing density variations with composition and between phases, allowing for expression of the relative volumes to be expected in a microstructure. This also includes the volume change between the liquid and solid phases and the attendant capillarity flow which this causes, of which inverse segregation is an extreme example.

The difference between the Scheil and lever rule predictions then appear as in Fig. 2 as C_s or C_L vs. $f_s = (1 - f_L)$, plotted in this case for a solid solution, terminating at a eutectic reaction. It is important to remember that for the lever rule, the solid composition, C_s, is that of the total, whereas for the Scheil plot, C_s is the local equilibrium solid in contact with liquid of uniform composition at any f_L or equivalent temperature. It is also common practice to plot the mean solid concentration for the Scheil prediction, $\bar{C}_s$, (see Fig. 1) on a phase diagram, in such a way as to express a non-equilibrium solidus which can be used as the basis for a modified lever rule balance where $\bar{C}_s$ only approaches C_o in the limit.

We then recognize, that the basic assumptions of no solid mixing, or of complete liquid mixing, implicit in the Scheil equation may need some relaxation and qualification, leading to segregation profiles intermediate between the two extremes of Fig. 2. Thus, either there may be only partial liquid mixing, or, more probably, there may be some back diffusion in the solid. In the context of microsegregation it is generally unnecessary to consider the case for limited liquid mixing, because the dimensions of local solidification volumes are typically well within $\sqrt{D_L t}$ (D_L = liquid diffusion coefficient and t is local solidification time - i.e. that time taken to cool from the liquidus to the final freezing point). Back diffusion in the solid, however, becomes a more serious problem, especially for alloys containing interstitial solutes - e.g. Fe-C. There have been semi-empirical (13,14) and more rigorous solutions to such back diffusion (15,16) which fit experimental microscopical and EMPA or other data with varying degrees of conformity (17,18,19).

It is pertinent to consider how close a fit to experimental results might reasonably be expected for these modified analyses.

Firstly, let us consider that EMPA data are based on multiple line trace analyses across microsections. However thorough or selective such data may be, they are still only line traces through local volumes which have solidified in three dimensions with continuously (or continually) changing geometrical phase distributions. The problem may be placed within any preferred reference coordinates, cubic or otherwise, but initially, the solidification consists of the thickening of dendrites, essentially the outward growth of cylindrical shapes, and then as these make contact there will be rapid adjustments of the morphology as the growth changes to radially inwards towards the centre of residual liquid droplets within a solid matrix (20,21). The Scheil equation, however modified, can only describe the

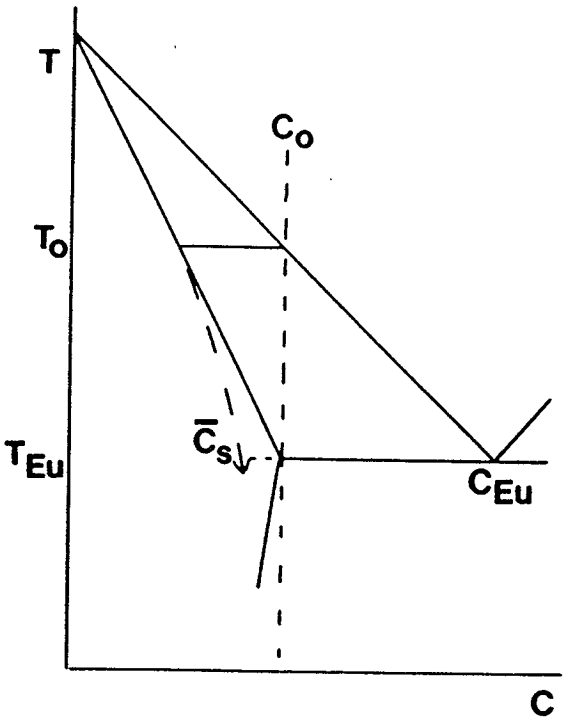

Fig. 1. Partial eutectic phase diagram with compositions and temperatures as in text and Figs. 2 and 3.

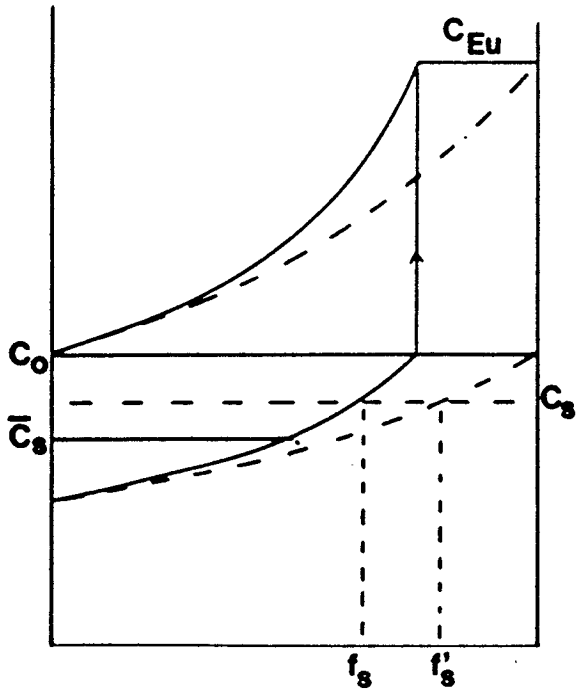

Fig. 2. Composition traces vs. fraction solid, f_s, for solidification of alloy, C_o, in Fig. 1, full lines according to Scheil, broken lines according to lever rule. $\bar{C}_s$ is the mean solid fraction, f_s and local composition, C_s; f's is the corresponding lever rule fraction.

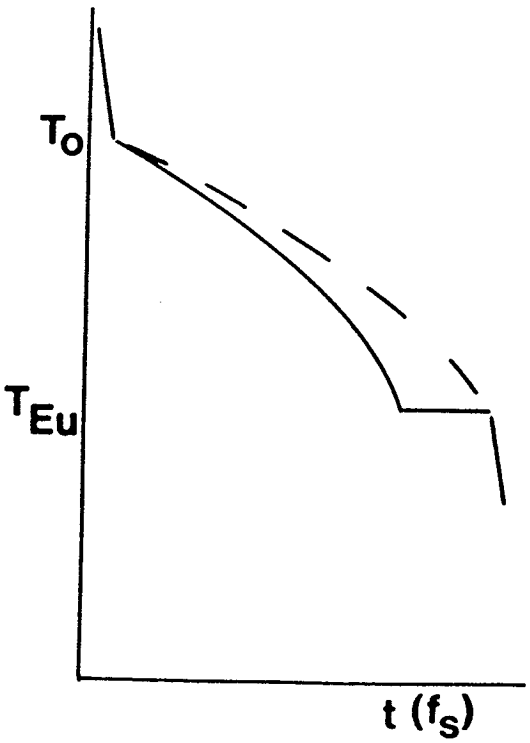

Fig. 3. Schematic cooling curves for a uniform rate of heat abstraction corresponding to alloy C_o, Fig. 1, full line according to Scheil, broken line according to lever rule.

relative masses or volumes of solid and liquid and cannot be expected, on a linear trace, to conform exactly with a changing geometrical distribution, which at longer times is also subject to coarsening and ripening adjustments. Unless this geometrical complexity can be adequately accounted for, precise agreement between analysis and observation cannot reasonably be expected, so that it is somewhat doubtful if this type of experimental data can be used to assess the relative merits of finer modifications to the Scheil equation.

However, in foundry practice, while subsequent and often detailed microanalysis may follow in the laboratory, a more direct, on line control is possible and easily accomplished through thermal analysis, either of isolated melt samples, or more elaborately, on model castings using multiple thermocouples. Given a realistic heat flow analysis, this approach requires that the lever rule or Scheil equations be transformed to a temperature scale vs. phase proportion, using the slope of the liquidus line or trace, if this is established or can be estimated - thus, corresponding to the composition vs. f_s plots of Fig. 2 we have the temperature vs. f_s plots of Fig. 3, i.e. the equilibrium and Scheil equivalent cooling curves for a given rate of heat abstraction. Clearly, also, there can be a continuum of intermediate forms for varying degrees of solid mixing. This is the only obvious direct method available to test solidification models against observation, but even given the ability to calculate local heat flow conditions, there remain other serious problems or unknowns arising from the columnar: equiaxed transition and the nucleation density. These are important, not only inasmuch as they concern the final grain structure but because they determine local growth rates, hence interface shape and the size of representative, local solidification volumes, and hence, the applicability of preferred segregation analyses. Arguments become circular and it is necessary to make arbitrary assumptions about the nucleation kinetics in order to "fit" analyses to observed cooling curves. The predictive capability is then sadly lacking unless nucleation sites can be identified and their surface potentials be quantified. At the present time this capability is generally lacking, except in a few cases where specific grain refining additions appear to operate, and even in these cases representation of the potency of surfaces is open to argument, e.g. for aluminum base alloys with Ti, B, etc. (22). Instead of attempting this imponderable problem, some progress has been made at 'curve fitting' to cooling curves of binary alloys, assuming the presence of unspecified nuclei of variable particle density and nucleation potencies, the latter expressed in terms of maximum undercoolings prior to recalescence (8,9). Examples of such comparisons appear in Fig. 4 and relate to (a), hypoeutectic Al-Si alloy and (b), to a cast iron. Both alloys contain primary dendrites and eutectic. The agreement between calculation and observation is similar in either case, but I suspect that by Weinberg standards they would not be hailed as entirely successful, but one might be optimistic and reflect that a start must be made somewhere.

In the absence of specific, identifiable nucleating substrates, the most probable and spontaneously efficient nucleation sites are from particles of the primary solid phase, either generated at low superheats on mold surfaces - so-called 'big bang' nucleation (23) - or arising by fragmentation of primary dendrites from the columnar zone at larger superheats (24); in the latter case, a mechanism must be considered for the transport of such fragments into the bulk liquid, where they may develop into equiaxed grains if the thermal conditions allow. Truly predictive modeling would require that such sources and the transport of crystal fragments be not only identified, but also quantified, and this may be the major obstacle to further useful progress. However, in the absence of induced or forced stirring of a melt, natural convection must provide the source of possible transport into and through the melt and it becomes immediately necessary to examine such convective patterns

and to recognize that they also determine solute redistribution on a macroscopic scale.

Aspects of Natural Convection and Macrosegregation

In any solidifying (or melting) material which exhibits a freezing range, liquid density gradients arise from both thermal and solutal gradients and interaction between these can lead to so-called thermo-solutal convective patterns (e.g. 25-30). Thus with respect to some reference axis or axes, there are thermal and composition gradients, dT/dz and dc/dz, which have associated density gradients, $d\rho/dz$, the magnitudes and senses of which depend upon the corresponding coefficients, $\alpha = d\rho/dT$ and $\beta = d\rho/dc$. α is always positive but β may be of either sign. Only for certain compositions in multi-component systems will $\beta \rightarrow 0$, in almost every binary system β is finite and is often such as to exceed α by an order of magnitude.

Since β may be of either sign, it is relevant to consider the geometrical configuration, i.e., whether growth is vertically upwards, antiparallel to gravity, $\uparrow\downarrow$, downwards, parallel, $\downarrow\downarrow$, or horizontal, i.e. at right angles to the gravitational vector, $\leftarrow\downarrow\rightarrow$. Schematically, Fig. 5, with a developed columnar mushy zone, these alternatives then allow the thermo-solutal contributions to combine or to oppose each other, depending on the sense of the g vector with respect to that of the temperature gradient, and upon the sign (and magnitude) of the solutal coefficient, β.

In a metallurgical context, identification of the buoyancy forces arising from solutal gradients came from directional growth studies (31) and in analogue castings (32,33) some twenty years ago, although it was recognized about the same time in oceanographic contexts (25,28,29) where it causes so-called thermo-haline convection effects. It is a generic effect applying to a wider range of natural phenomena, including geological situations (34).

With constrained growth into positive temperature gradients, composition variations occur between the bulk and interdendritic liquids and at the dendritic growth front itself: the corresponding density gradients then interact with the thermal density variations as shown, Fig. 5(a)-(f). Thus, with horizontal growth (a), β negative, there is a buoyancy force tending to cause flow upwards and with β positive, (b), a reverse tendency, such that in each case, excess solute accumulates at the top or bottom of the ingot, and, with depression of the freezing point, $k_o < 1$, this distorts the growth front accordingly, as indicated. With vertical growth upwards, (c) and (d), the solutal contribution is opposed to the stabilizing thermal field, with β-negative, or reinforces it and maintains a quiescent liquid above and below the growth front, (d). The situation in case (c) is of particular interest because the incidence of convection is not spontaneous, even if the destabilizing solutal density gradient exceeds that from the temperature gradient. this situation has received much experimental and theoretical attention. Lastly, in (e) and (f), the bulk liquid is continuously mixed by the inverted thermal field to which the solutal contribution may be either opposed, (e), or will reinforce such convection, (f), as more dense solute seeks to flow downwards into the bulk liquid.

Convective flow is continuous and circular, i.e., that which goes up must come down since fluids are effectively incomprehensible, although they expand with temperature - a so-called Businesque fluid. Within and without the dendritic array of a mushy zone, the continuity of convective flow is naturally accomplished by the formation of localized channel patterns. In the bulk liquid these localized flows exist as streamlined, solute rich plumes, ~ 1 mm wide and $\geq 10^2$ mm long, emanating from the growth front. Evidence of their existence remains behind in the fully solidified material as channel segregates - well known casting defects, 'A' segregates in steel billets (e.g. 10,35,36) or 'freckles' in directionally solidified E.S.R. ingots or

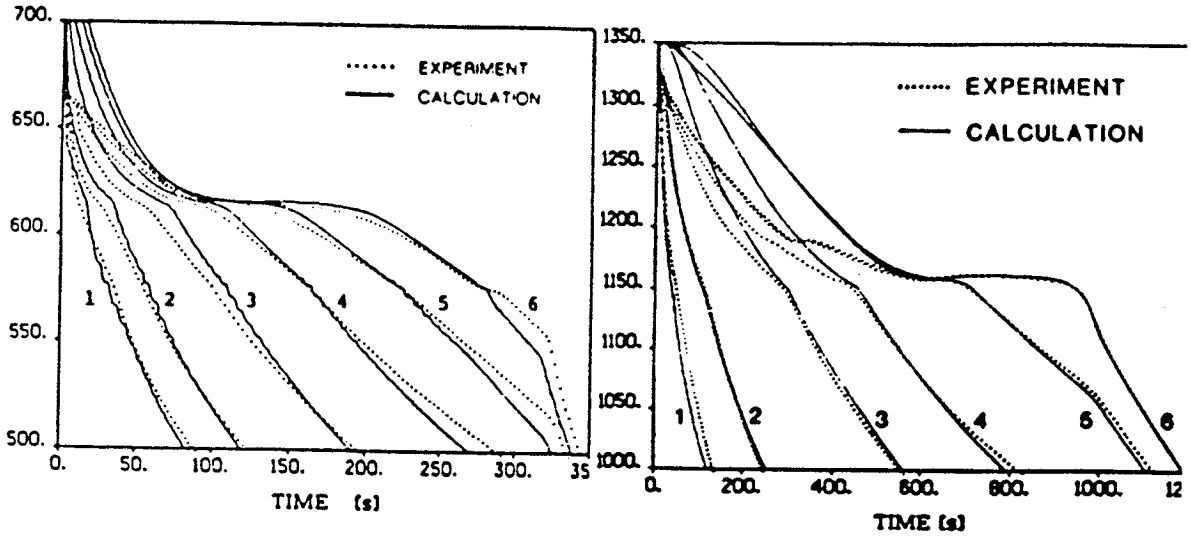

(a) (b)

Fig. 4. Calculated and experimental cooling curves for six position in samples of (a) Al-7 wt.% Si and (b) hypoeutectic cast iron, after refs. 8 and 9.

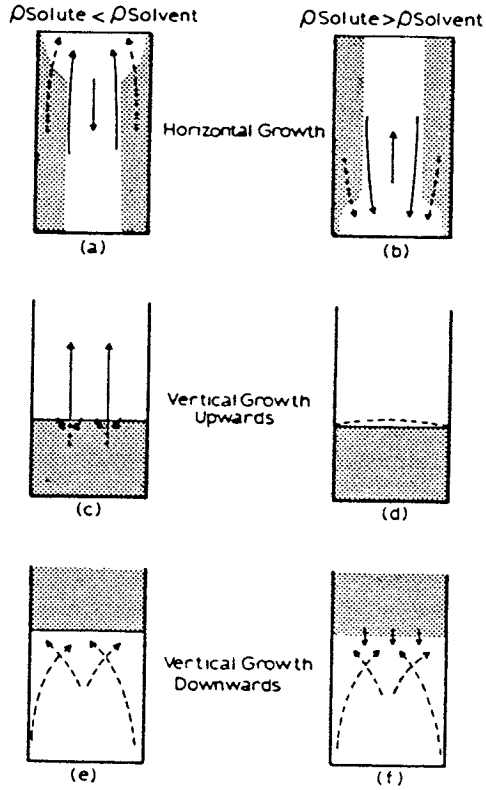

Fig. 5. Schematic convective patterns during alloy solidification with shaded 'mushy zones'. (a) growth normal to gravitational vector, g, $\leftarrow^{\downarrow}\rightarrow$, $\Delta\rho-$; (b) the same with $\Delta\rho+$; (c) growth upwards, antiparallel to g, $\uparrow^{\downarrow}$, $\Delta\rho-$; (d) the same with $\Delta\rho+$; (e) growth downwards, parallel to g, $\downarrow\downarrow$, $\Delta\rho-$ and (f) the same with $\Delta\rho+$.

superalloy turbine blades (37). Such channels can be found in the configurations (a), (b), (c), and (f) of Fig. 6 and they certainly offer one mechanism by which dendrite crystal fragments are transported from the mushy zone into the bulk liquid. However, in billet castings, (a) and (b), and with downwards growth, (f), such patterns are combined with other bulk fluid flows and are more difficult to study. That is why most attention has focused upon the particular configuration of Fig. 5(c), where interdendritic liquid exhibits density inversion but is surmounted by quiescent bulk liquid which is stabilized against convection by the positive temperature gradient. It is the manner in which this less dense, interdendritic liquid escapes into the more dense bulk liquid which is particularly interesting and instructive, causing a special type of thermo-solutal convection.

Figure 6 summarizes this situation. An alloy of composition C_o solidifies vertically upwards into a positive temperature gradient, dT/dz. At the dendritic front there is a slightly enriched boundary layer at C_L, depositing solid C_D, while between the dendrites the liquid is in local equilibrium with the solid according to the temperature and composition along the liquidus line. If β x dc/dz exceeds α x dT/dz, along the liquidus, the density gradient below the growth front is positive, i.e. the system exhibits density inversion and is inherently unstable. However, although this positive gradient often exceeds the negative, thermally controlled density gradient above, perturbations leading to some form of convection do not occur spontaneously because of a finite viscosity and the thermal inertia of the system. We note that $D_{thermal} >> D_{solute}$, so that while a perturbation may be able to achieve near thermal equilibrium in a short time, solute diffusion is so slow that there is insufficient time for composition adjustment. It has then been of recent interest to identify where and when these convective channels develop and, subsequently, to understand, what determines their flow rates and spacings. The following relates to the vertical case of Fig. 5(c).

(i) Position of Origin

The choice here is from a site within the partially solid mushy zone or elsewhere, such as at the growth front or above that front in the bulk liquid. Although analyses have been formulated for the former origin (38-40), experimental evidence (41-42) suggests that the convection starts at or immediately ahead of the dendritic front. The observations which indicate this site preference are (a), direct studies of the transparent aqueous system NH_4Cl-H_2O, which reveal that channels within the mushy zone originate from local disturbance of liquid close to the front and then spread back (i.e. downwards) into the partially solid region; (b) artificial creation of channels, by boring holes into the mush region, does not, per se, lead to self perpetuating channel plumes, but, the artificial creation of upward plumes in the bulk liquid, ahead of the growth front does result in the formation of coincident channels and self sustained plume flows; while, (c), mold movements which cause the bulk liquid to sweep across the front will inhibit the development of local convective flows or stop any which have developed. These experimental procedures are summarized in Fig. 7(a)-(c).

In retrospect, it is obvious that channel mouths and established plumes are part of a continuous flow pattern and the one cannot exist without the other, but the most probable level at which these will originate is where the sign of the density gradient reverses. Without perturbation at this level, fluid movements at greater depths cannot be released; it is at this level that the less dense liquid needs to break through into the quiescent, supernatant bulk. In a sense, this level is an interface, although a diffuse one.

There is presently no formal analysis of this break away of the boundary layer fluid. The positions on the front have not been seen to be associated

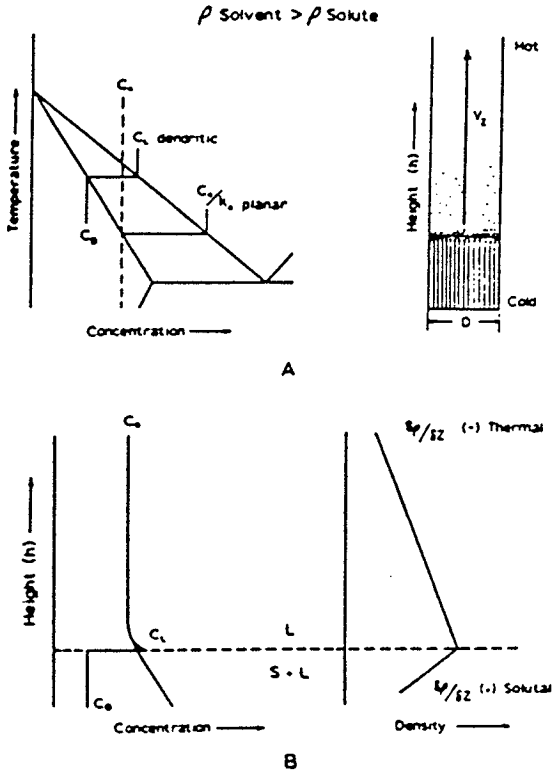

Fig. 6. (A) Conditions as for Fig. 5(c), initial concentration C_o, local liquid concentration at dendrite tips, C_L, (B) expected liquid concentrations above the growth front, $C_L \rightarrow C_o$, and below the front between primary dendrites of solid composition C_D.

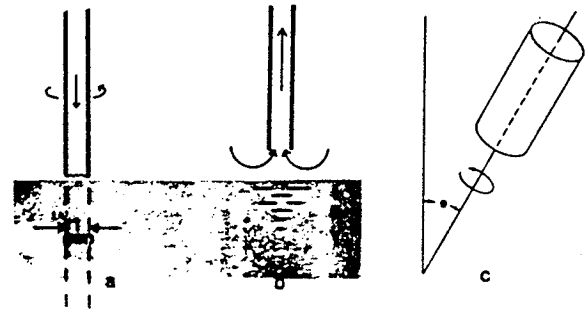

Fig. 7. Schematic representation of experiments relating to origin of channels, (a) artificial drill of a channel, (b) artificial creation of a plume above the growth front and (c) mode of precessional movement which eliminates channels and plumes.

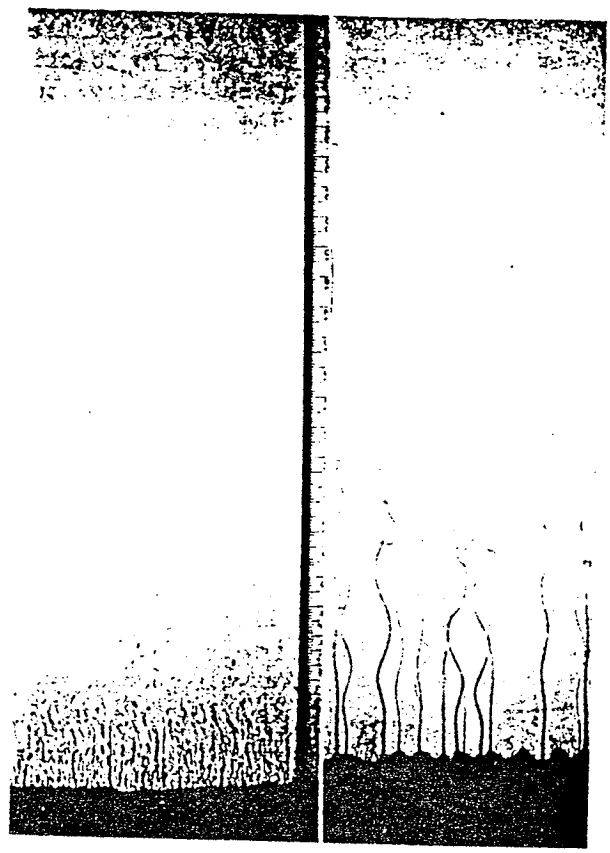

Fig. 8. 'Finger' and 'plume' convection patterns above an aqueous NH_4Cl growth front (courtesy of C. F. Chen).

with defects in the dendritic array, such as grain boundaries. A simple minded analysis of the quantities in a critical Rayleigh number (43) show that if this number were unity, the relevant dimension in the equation, in both metallic and aqueous systems, could be the primary interdendritic spacing. Indeed, since the liquid perturbation is occurring at such a periodic front, this coincidence might well be expected.

For a given alloy, in a given system, the primary dendritic spacing is a function of the imposed temperature gradient, G, and the growth rate, V (approximately proportional to $G^{-1/2}$ $V^{-1/4}$ (e.g. 11)) and while the former also influences the buoyancy gradients, it might be expected, and is qualitatively observed (37,44), that steeper temperature gradients and higher growth rates, which refine the primary spacing, also reduce or inhibit the incidence of segregation channels.

The incidence of channels is also composition dependent, inasmuch as this influences the liquid fraction and permeability of the mushy region; there appears to be a lower composition/permeability limit below which channels do not occur, for a given buoyancy pressure and Prandtl number, and an upper level where single channels and plumes are not observed. Above these upper levels, individual plumes and channels are replaced by a regime of smaller fluctuating 'fingers' on a similar scale to that of the primary dendritic spacing, Fig. 8. The transitional coupling between initial 'finger' perturbations and well defined, wider, quasi-steady state plumes is not well understood. At present, we are not able to predict, except in a very qualitative manner, when long range channel flows will develop.

(ii) Channel Plumes and Their Dimensions

As previously noted, the propagation of quasi-steady-state channel plumes is separate and subsequent to the initial perturbation. There are (at least) six relevant and interrelated, first order quantities involved in this problem; these are listed in Table I, although not necessarily in any selective order.

To these, it may also be relevant to consider second order quantities, including (a) temperature gradient, dT/dz, (b) growth rate, (c) height of mushy zone (d) height of meniscus above the latter and (e) width of container.

Many of these quantities have been measured (Table II) (43,44), including systems from materials having significantly different physical properties. These properties are conveniently defined by the dimensionless Prandtl and Lewis numbers, σ and τ. The systems are metallic Pb-Sb, Pb-Sn and ternary Pb-Sb-Sn, aqueous NH_4Cl and organic succinonitrile (SCN)-ethanol. Some of the quantities cannot be measured in all cases, notably the flow rates in opaque metals, and indeed, it is one of the objects of the research to estimate this quantity by extrapolation from other transparent systems. There are also some uncertainties or margins of error (e.g. $\pm$ 10%) in some of the measurements. Thus, precise channel or plume "widths" need to be defined and measured flow rates in the transparent materials are not necessarily maximum axial rates. Moreover, channel/plume compositions are averages, based on EMPA (Pb-base) or direct sampling and refractive index measurements for the aqueous and organic materials.

The outstanding question which then arises is, "how does the system select these quantities"?

One approach is to examine the plume flow in order to understand how the width, velocity and buoyancy forces are tied together.

The plume flow may be first considered as flow along a tube without constraints at either end. If a 'no slip' condition applied at the tube

TABLE I
Relevant Data

(i) Channel width (to be defined) - radius R_o
(ii) Flow rate (mean or maximum) - w
(iii) ΔC (plume vs. bulk) vs. time and position
(iv) ΔT (plume vs. bulk) vs. time and position
(v) Mean spacing, L
(vi) Permeability of mushy zone (primary and secondary spacings, λ, and fraction liquid, f_L)

TABLE II
Present Data Available

	Metallic	Aqueous	Organic
σ	$\sim 2\ 10^{-2}$	~ 7	~ 30
τ	$\sim 3\ 10^{3}$	$\sim 10^{2}$	$\lesssim 10^{2}$
Width	✓	✓	✓
Velocity	*	✓	✓
Composition	✓	✓	✓
Temperature	*	✓	✓
Spacing	✓	✓	✓
Permeability	✓	✓	✓

*No measurements

walls, flow along it would adopt the usual parabolic velocity distribution as in Poiseuille. However, this is not exactly the case because the 'walls' do not have a specific interface but rather represent a region of rapid shear, liquid without the tube being dragged upwards by the internal buoyancy, therefore having an exponential, radial velocity distribution around the plume. At some radius, the internal and external velocity distributions coincide at a common dw/dR Fig. 9; this is one way of identifying the effective plume width, i.e. where $d^2w/dR^2 = 0$. In a transparent material this is the position where the refractive index changes most rapidly and corresponds to a 'width' which is detected optically. The velocity distribution then fits a modified parabolic distribution of the basic form:

$$w = \frac{P R_o^2}{2h\eta}$$

where R_o is the effective plume radius, h is the plume height, P is pressure, of the form $\Delta\rho$ g h, and η is the dynamic viscosity coefficient. It will be seen that the density difference, $\Delta\rho$ is then given by $\beta\ \rho\ \Delta C$, involving the solutal coefficient, β, and the (mean) composition difference, ΔC, between plume and surrounding bulk liquids. This buoyancy pressure may be reduced if the plume liquid temperature remains below that of the bulk (which it does by 0 - 4K) by a term $\alpha\ \rho\ \Delta T$.

Combining these contributions for the aqueous system on a plot of w vs. R, Fig. 10(a) and (b), then shows that the parabolic function passes through the small scatter of experimental results which lie around $w \approx 7$ mm s^{-1} at $R \approx 0.6$ mm. Similar agreement is obtained for the organic data, and extrapolating the model for measured ΔC and R values would then indicate extremely rapid metallic plume flow rates exceeding 100 mm s^{-1}!

But, we still lack a criterion for this selection process. Two possibilities might be considered: one, that the plume flow be as rapid as is

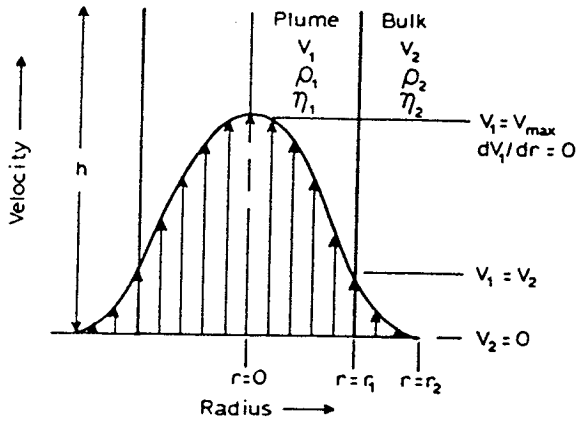

Fig. 9. Schematic velocity profile across a convective plume - refer to text.

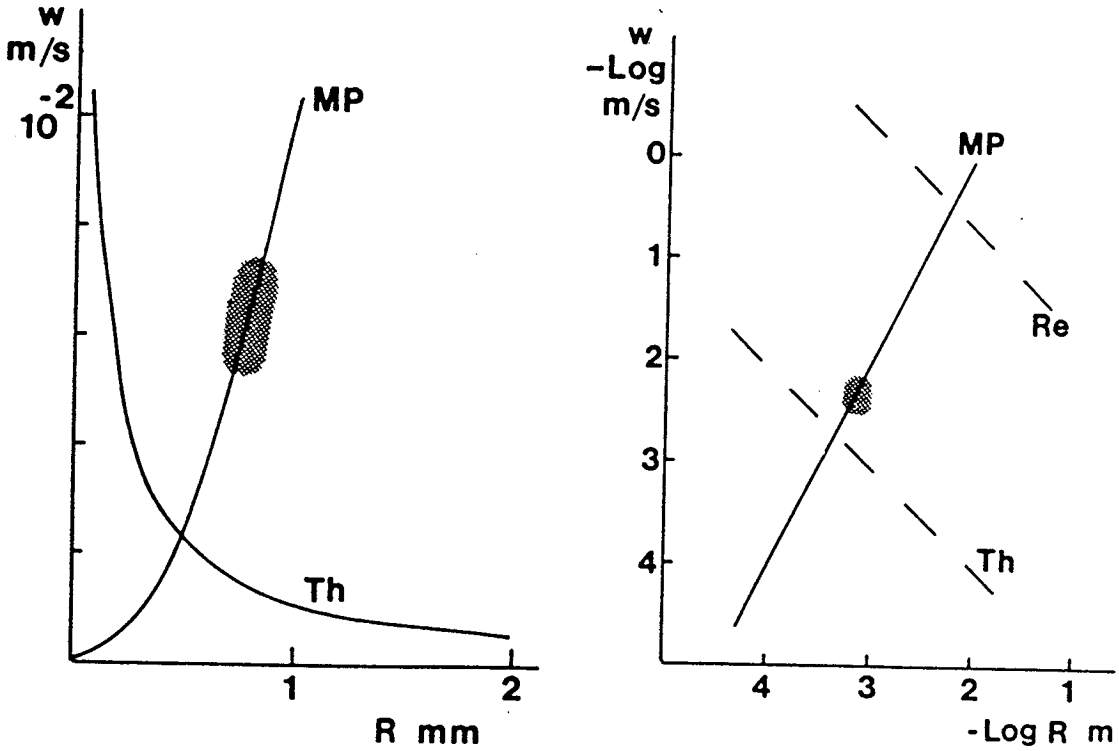

Fig. 10. (a) plot of plume flow velocity, W, vs. radius, R, shaded area includes experimental observations, MP is predicted by a modified Poiseuille equation, Th is a limit for thermal equilibrium, $W = \kappa/R$, (b) corresponding logarithmic plot including turbulence limit for Reynolds #, Re = 1000, $W = Re/R$. Data for NH_4Cl-H_2O.

consistent with streamlined flow - i.e. lies within the onset of turbulence, or, two, that flow occurs at such a rate, along plumes of such a dimension, as to allow the plume liquid to continuously adjust to the temperature of the surrounding bulk liquid. This is the condition which applies to a steady state perturbation in the first place.

For the first of these alternatives, the flow rate, tube radius and kinematic viscosity, ν, should fall within the limits of a critical Reynold's number:

$$Re = w\ R/\nu$$

where ν is the kinematic viscosity, η/ρ. The transition from laminar to turbulent flow is known to occur at a critical value of $Re \gtrsim 10^3$, so that we may write:

$$w = Re\ \nu/R$$

and trace this upon the same plot of w vs. R in Fig. 10(a). Inserting data for the aqueous solution yields a turbulence limit some three orders of magnitude greater than experimental data, so that it can only be compared on a logarithmic scale, Fig. 10(b). This cannot be a relevant consideration and the observed rates and dimensions are entirely within the streamline regime. The same is true for the organic example and even in the metallic case the turbulent regime would still lie beyond our extrapolated value of velocity, by a factor of ~ x 5.

The second criterion, for thermal equilibrium, would require that the plume radius were close to κ/w, or $w \approx \kappa/R$. This limit also appears on Figs. 11(a) and (b), and as may be seen, it falls below the observed range by about an order of magnitude. This means that the plume flow is not only much too rapid for there to be any composition change, but that it is also too fast to allow thermal equilibrium to be achieved: fine thermocouples, moved through plumes, confirm this conclusion.

Insertion of data for the metallic and organic materials leads to the same conclusion, although in the metal we have no confirmatory temperature measurements - it is virtually impossible to find a plume in an opaque liquid, except by accident and inference. Neither criterion seems to offer a controlling limit.

It is pertinent to reexamine the previous assumption that the plume flow is unconstrained at either end, in particular, the limits on supply of entrained liquid around the channel which exits at the base of a plume, Fig. 11. This is a geometrical problem which is imposed by the fluid viscosity and the permeability of the mushy zone. These control the volume of fluid which can be drawn through (be entrained into) the mushy region surrounding a channel exit, at and below the growth front, i.e., the base of the plume is effectively embedded in a filter.

For a plume to be able to operate it is necessary to consider the number, N, of interdendritic pipes, of radius, r, which feed into the channel circumference, and to what depth below the front this supply is significant. It is also necessary to consider how long the pipes are and how rapid is the entrained flow rate along them. Estimates and measurements can be and have been made (e.g. 42,44). Clearly, there is a lower limit to the porosity/permeability of the dendrite mesh for a given buoyancy pressure, below which the necessary entrainment cannot be sustained. This, in a simplified form, can be expressed in terms of the fraction liquid in the mushy zone at some level, f_L, the channel radius, R, and its ratio to the primary interdendritic spacing, λ, this last dimension being the superimposed grid dimension to which all dimensions can be referred, i.e.

$$f_L \bar{>} R^m/A\,\lambda^n$$

where A is geometrical term, $m \approx 3/2$ and $n \approx 1$. It will be understood that there is some latitude within the term A depending upon the choice of a realistic model for the entrainment pattern. The limiting fraction of liquid also applies at some depth below the growth front, related to the term, A. Since f_L is composition dependent, there is, understandably, a lower critical value for channel/plume formation in any system.

(iii) Other Configurations

We conclude, from the preceding, that the factors controlling perturbation of the boundary layer region are separate from those which allow the larger scale plume/channel flow to be sustained. There can be fine scale fingers without fully developed plumes, Fig. 8. The situation might be compared with conditions allowing plane front breakdown vs. those governing subsequent growth forms.

All this discussion was in the context of a configuration where growth occurs vertically upwards, c.f. Fig. 5 (c), with density inversion below the growth front. Some comments on the other alternatives are in order, particularly with side chill geometry and horizontal growth, as in billet castings, Fig. 5(a) or (b). There is also the problem of what might be expected with continuously changing inclinations, as during continuous casting operations.

With a vertical, or near vertical growth front the situation is modified by convection patterns in the bulk liquid and parallel to the front. These arise, in part, because the solute boundary layer at the front is more or less dense than the bulk and so causes a downward or upward stream which precedes channel formation and is probably more important as a means of transporting solute and crystal fragments within the melt. In the bulk liquid, at some distance from the solute boundary layer, the bulk liquid may also exhibit thermally induced convection patterns with downward flow at the sides, in opposition to the solutal convection for a less dense solute. Channels do develop however, as 'A' segregates and are not only restricted to the upward or downward facing parts of the front which reflect macroscopic solute accumulations. It is not altogether clear whether formation of these channels is assisted or damped by the bulk liquid movements. On the one hand, there is no boundary layer perturbation needed as there was in the previous case, $\uparrow^{\downarrow}$, because the fluid ahead of the front is already being swept along in the same direction as any potential plume flow. On the other hand, we know that in that other configuration a circular or processional motion will inhibit or eliminate plume and channel formation.

Visual examination of transparent analogues is somewhat ambiguous in this respect, but one interesting feature does appear and seems to arise from the upward (or downward) flow over the dendritic front, causing rivulets or streams to develop in the plane of the front, Fig. 12. It is possible that channels develop from these grooves and/or that they become incorporated in the mushy zone and are partially or completely overgrown. This action will enhance the fragmentation of dendrites and be an efficient source of potential equiaxed grains. The effect is enhanced if the growth front is slightly inclined and overhangs the bulk liquid, so it may well assume more importance in continuous casting of steels as the strand bends away from the vertical.

The convective patterns are very sensitive to quite small inclinations away from the vertical - e.g. by as little as 5° - and can then change from symmetrical to asymmetrical distributions. Associated with such inclinations, in continuous steel castings around the peritectic range, notably but not exclusively with curved molds, the columnar:equiaxed grain distribution becomes asymmetric, such that the columnar length on the overhanging, inner

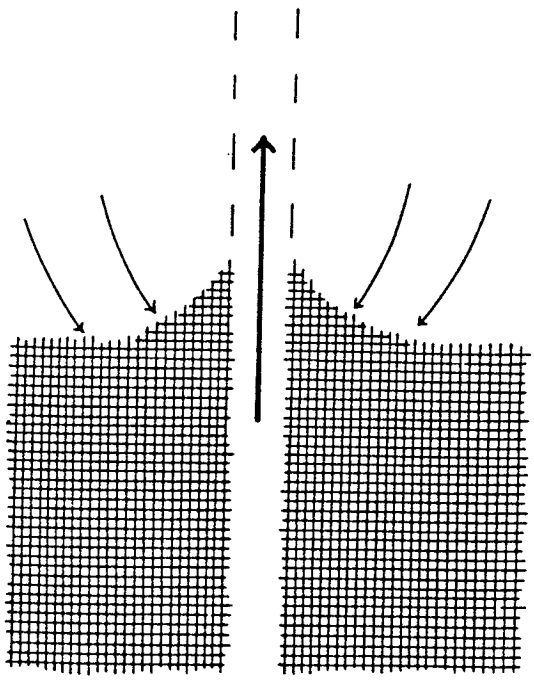

Fig. 11. Schematic representation of local growth front around channel mouth.

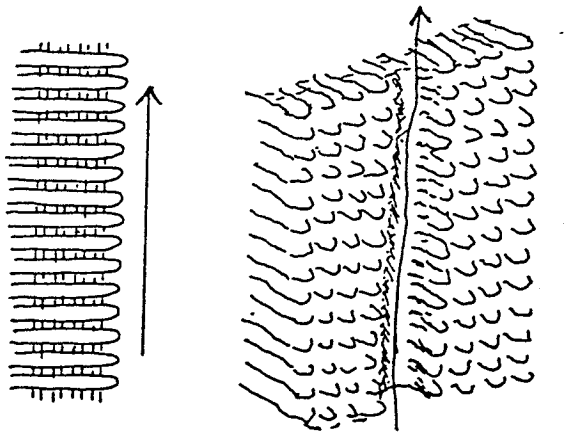

Fig. 12. Type of rivulet flow which can develop at a vertical dendritic growth front, $\Delta\rho$-, as in Fig. 5(a).

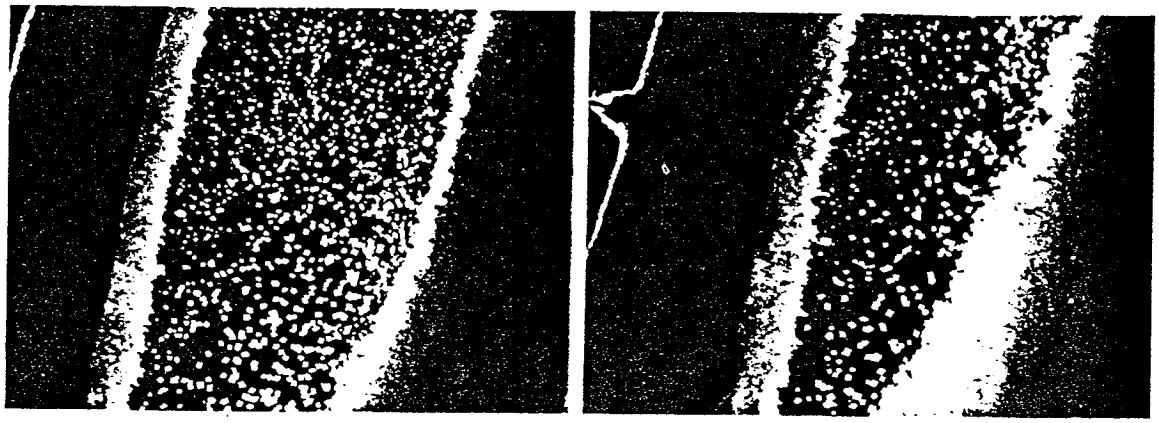

(a) (b)

Fig. 13 (a) and (b). Showing development of an asymmetric grain structure in an NH_4Cl-H_2O analogue casting with an inclined mold, time interval 4 minutes (courtesy of Jinsung Jang - to be published).

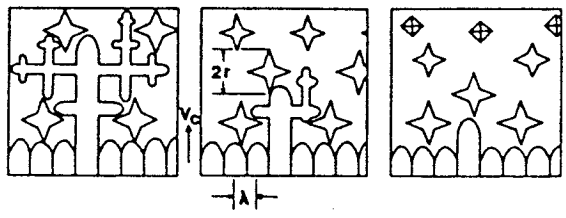

Fig. 14. Schematic representation of the blocking of a columnar front by falling equiaxed crystals.

To effectively block the columnar dendritic front it will be necessary to deposit a second row of grains BEFORE the dendritic front has advanced beyond the first layer.

side of the strand is longer than that on the lower, outer side (e.g. 46). This development has been reasonably attributed (47) to the formation of crystal fragments which grow and fall through the bulk liquid, away from the overhanging front eventually accumulating on the lower front and blocking further columnar growth. This can be visually demonstrated with an analogue casting of NH_4Cl-H_2O, as in Fig. 13(a)-(b). This raises one further problem for which we need a realistic model, namely, what criterion should be accepted for a columnar blocking mechanism? The problem requires consideration of the density of falling crystallites, and therefore their origin at higher levels in the casting, their growth and sedimentation rates and the rate of arrival at the dendritic columnar front, necessary to effectively block that front. There have been a number of models presented for this situation (48,49), essentially involving the arrival of sedimenting, equiaxed crystals upon the front, at such a rate that the columnar dendrites cannot grow between these obstacles in less time than another layer arrives. Fig. 14 depicts the geometrical configuration for a horizontal front, growing upwards. For an inclined, or indeed for a vertical front, further complications arise from a need to invoke a sticking coefficient or 'piling up' arrangement from some lower level, such as from the base of a billet casting or some critical level in a continuously cast strand.

Summary and Conclusions

Necessarily, this has been a rather selective review of various aspects of segregation during alloy solidification. The object was to identify some of the parts of the overall picture which are still in need of interpretation if the casting process is to be modeled in a realistic and predictive manner. Emphasis is laid upon 'predictive', as opposed to 'curve fitting', as of cooling curve data, although it is recognized that the latter practice may represent a necessary preliminary exercise. The following points were discussed in more or less detail:

(i) Analyses for fractional crystallization and solute redistribution during solidification have been developed in some detail for different extents of solid diffusion. These analyses can obviously be applied to describe microsegregation but the complexities of shape changes in the solid-liquid range make precise experimental confirmation difficult.

(ii) Given the necessary information about the relevant phase equilibria (solid-liquid distribution coefficients and liquidus data), coupled with realistic heat flow analysis, the solute mass balance can be transformed to a temperature scale in order to calculate a cooling curve.

(iii) This approach must be set in a context of a casting, incorporating a description of the columnar to equiaxed transition and of the nucleation process leading to the development of equiaxed grains. Information of this type is necessary to identify the scale of local solidification volumes within which the solute redistribution must be predicted.

(iv) The most probable and efficient sources of nuclei are fragments of the solid material, either swept off chill surfaces ('big bang') or transported from the columnar region by convection or other induced stirring. In the latter case it becomes necessary to consider how liquid density variations develop in temperature and composition gradients.

(v) Thermo-solutal convective patterns in the form of channel/plume flows were described, particularly as they develop at a dendritic growth front growing vertically upwards. The origin of these was discussed and the factors controlling their flow rates and dimensions were considered; it was concluded that the permeability of the mushy zone is the major controlling factor. Reference was made to observations of metallic, aqueous, and organic materials.

(vi) In other geometrical configurations with horizontal growth, or with continuously changing inclination to the vertical, bulk liquid convective movements probably override channel patterns as a means of transporting crystal nuclei.

(vii) To complete the picture of the overall process it is necessary to return to the need for a model to describe how falling equiaxed crystals block a dendritic columnar growth front in different configurations.

It will be necessary to develop physically realistic models for all these aspects if truly predictive analysis of ingot solidification is ever to be accomplished.

Acknowledgments

The description of channel convection was largely based on recent work by J. R. Sarazin at MTU, being part of a program supported by NASA, grant #NAG-3-560 and by the NSF Division of Materials Research, grant DMR-8815049.

References

1. Modelling of Casting and Welding Process I, (H. D. Brody, D. Apelian, eds.), The Metallurgical Soc. AIME, 1981.
2. Modelling of Casting and Welding Processes II (J. A. Dantzig, J. T. Berry, eds.) The Metallurgical Soc. AIME, 1984.
3. W. Oldfield, Trans. ASM, 59, 945 (1966).
4. I. Maxwell and A. Hellawell, Acta. Met., 23, 229 (1975).
5. W. C. Winegard and B. Chalmers, Trans. ASM., 46, 1214 (1953).
6. S. C. Flood and J. D. Hunt, Applied Science Res., 44, 27 (1987).
7. R. B. Mahapatra and F. Weinberg, Met. Trans. B, 18B, 425 (1987).
8,9. M. Rappaz and Ph. Thévoz, in Solidification Process, 1987, The Institute of Metals, Book #421, p. 164 and p. 168.
10. M. C. Flemings, Solidification Processing, McGraw-Hill, 1974.
11. W. Kurz and D. J. Fisher, Fundamentals of Solidification, Trans. Tech. Publications, Aedermannsdorf-Switzerland, 1986.
12. E. Scheil, Zeit. f. Met., 34, 70 (1942).
13. H. D. Brody and M. C. Flemings, Trans. Met. Soc. AIME, 236, 615 (1966).
14. T. W. Clyne and W. Kurz, Metall. Trans., 12A, 965 (1981).
15. M. Rappaz and V. Voller, Metall. Trans., 21A, 749 (1990).
16. K. S. Yeum, V. Laxmanan, and D. R. Poirier, Metall. Trans., 20A, 2847 (1989).
17. H. Thresh, M. Bergeron, F. Weinberg and R. K. Buhr, Trans. Met. Soc. AIME, 242, 863 (1968).
18. F. Weinberg and E. Teghtsoonian, Metall. Trans., 3, 93 (1972).
19. F. Weinberg, Trans. Met. Soc., AIME, 221, 844 (1961).
20. A. Hellawell, The Solidification of Metals, Iron and Steel Institute, London, ISI Publication 110, 83 (1968).
21. R. M. Sharp and A. Hellawell, J. Crystal Growth, 11, 77 (1971).
22. A. Hellawell, Solidification and Casting of Metals, The Metals Soc., London, Book 192, p. 161 (1979).
23. B. Chalmers, Principles of Solidification, Wiley, New York, 1964.
24. K. A. Jackson, J. D. Hunt, D. R. Uhlmann, and T. P. Seward, Trans. Met. Soc. AIME, 236, 19 (1966).
25. M. E. Stern, Tellus, 12, 172 (1960).
26. G. B. McFadden, R. G. Rehm, S. R. Coriell, W. Chuck and K. A. Morrish, Metall. Trans., 15A, 2125 (1984).
27. S. R. Corriell, M. R. Cordes, W. J. Boettinger, and R. F. Sekerka, J. Crystal Growth, 49, 13 (1980).
28. R. W. Schmitt, Phys. Fluids, 26, 2373 (1983).
29. J. S. Turner, Rev. Fluid Mechanics, 17, 11 (1985).
30. H. Huppert, J. Fluid Mechanics, 212, 209 (1990).

31. N. Streat and F. Weinberg, Metall. Trans., 5, 2539 (1974).
32. R. J. MacDonald and J. D. Hunt, Trans. Met. Soc. AIME, 245, 1993 (1969).
33. S. M. Copley, A. F. Giamei, S. M. Johnson, and M. F. Hornbecker, Metall. Trans., 1, 2193 (1970).
34. H. E. Huppert, J. Fluid Mech., 173, 557 (1986).
35. G. J. Davies, Solidification and Casting, Applied Science, London, 1973.
36. F. Weinberg, J. Lait, and R. Pugh, Solidification and Casting of Metals, The Metals Society, London, Book 192, p. 334 (1979).
37. A. F. Gaimei and B. H. Kear, Metall. Trans., 1, 2185 (1970).
38. M. R. Bridge, M. P. Stephenson, and J. Beech, Metals Technology, 9, 429 (1982).
39. V. R. Voller, J. J. Moore, and N. A. Shah, Metals Technology, 10, 81 (1983).
40. M. Simpson, M. Yerebakan, and M. C. Flemings, Metall. Trans., 16A, 1687 (1985).
41. A. K. Sample and A. Hellawell, Metall. Trans., 13B, 495 (1982).
42. A. K. Sample and A. Hellawell, Metall. Trans., 15A, 2163 (1984).
43. J. R. Sarazin and A. Hellawell, Metall. Trans, 19A, 1861 (1988).
44. J. R. Sarazin, Ph.D. Thesis, Mich. Tech. Univ., 1990.
45. S. K. Morton and F. Weinberg, J. Iron and Steel Inst., 211, 13 (1973).
46. J. E. Lait, J. K. Brimacombe, and F. Weinberg, Iron and Steelmaking, 1, 36 (1974).
47. R. Bommeraju, J. K. Brimacombe, and I. V. Samarsekera, Trans. Iron and Steel. Soc., 5, 95 (1984).
48. F. Weinberg, Metall. Trans., 15B, 479 (1984).
49. S.G.R. Brown and J. A. Spittle, Metal. Sci. and Tech., 362 (1989).